Canadian Science Publishing | Canadian Journal of Microbiology

The *Campylobacter fetus* S layer provides resistance to photoactivated zinc oxide nanoparticles.

Journal:	*Canadian Journal of Microbiology*
Manuscript ID	cjm-2018-0451.R1
Manuscript Type:	Article
Date Submitted by the Author:	22-Feb-2019
Complete List of Authors:	Graham, Lori; St. Francis Xavier University, Biology Feero, Stephanie.E.; St. Francis Xavier University
Keyword:	Campylobacter fetus, S layer, Zinc oxide nanoparticles, reactive oxygen species (ROS)
Is the invited manuscript for consideration in a Special Issue? :	Not applicable (regular submission)

The *Campylobacter fetus* S layer provides resistance to photoactivated zinc oxide nanoparticles.

Submitted to the Canadian Journal of Microbiology

L.L. Graham* and S.E. Feero†
Department of Biology
St. Francis Xavier University
Antigonish, NS, B2G 2W5

*author to whom correspondence should be addressed
Email: lgraham@stfx.ca
Telephone: 902-867-2386

†current address:
Email: stephaniefeero@gmail.com

ABSTRACT

The antimicrobial activity of metal based compounds, including metal oxides, has resulted in numerous agricultural, industrial and medical applications. Zinc oxide nanoparticles are toxic to gram positive and gram negative bacteria as well as to some fungi. In this study we assess the sensitivity of *Campylobacter fetus*, a gram negative bacterial pathogen of humans and animals, to ZnO nanoparticles and determine whether the S layer protects *C. fetus* from the antibacterial action of these nanoparticles. Broth and agar dilution assays revealed that ZnO nanoparticles at 100 μg/mL were bacteriocidal for *C. fetus*. Resazurin reduction assays confirmed the absence of metabolic activity, indicating that *C. fetus* cells had not entered into a viable but non culturable state. Photoactivation of ZnO nanoparticles greatly enhanced their antibacterial activity as evidenced by Minimum Bacteriocidal Concentration (MBC) values decreasing to 16 - 62.5 μg/mL as a function of strain. MBC assays completed in the presence and absence of catalase revealed that H_2O_2, a product of ZnO nanoparticle photoactivation, contributed to *C. fetus* but not to *C. jejuni* cell death. S layer expressing *C. fetus* strains were more resistant to H_2O_2 mediated cell killing than were isogenic S layer deficient strains. This data indicates that *C. fetus* is sensitive to the antibacterial activity of ZnO nanoparticles and that the *C. fetus* S layer imparts protection against photoactivated nanoparticles.

Keywords: *Campylobacter fetus*, S layer, ZnO, nanoparticles, reactive oxygen species

Introduction

The genus *Campylobacter* comprises more than 26 species of gram negative, spiral shaped bacteria. Reservoirs for these organisms include the intestinal microbiota of many animals and the oral microbiota of humans. Of the 17 *Campylobacter* species associated with human infection, *C. jejuni* is most frequently isolated (Kaakoush et al. 2015). *C. fetus,* in contrast is more often considered to be a veterinary pathogen, though human infection occurs. *C. fetus* has 3 subspecies, *C. fetus* subsp. *testudinum*, normally associated with reptiles (Gilbert et al. 2014), as well as *C. fetus* subsp. *venerealis* and the closely related *C. fetus* subsp. *fetus*. Recent genomic analyses reveal that *C. fetus* subsp. *fetus* and *C. fetus* subsp. *venerealis* are highly syntenic, sharing 92.9% sequence identity. The remaining unique genomic regions contribute to the host tropism observed in these two subspecies. *C. fetus* subsp. *venerealis* is a bovine adapted pathotype causing venereal disease in cattle, whereas *C. fetus* subsp. *fetus* strains are adapted either to an ungulate host (typically cattle, sheep and goats) or to humans (Kienesberger et al. 2014). Both human and ungulate *C. fetus* subsp. *fetus* pathotypes are associated with extra-intestinal infection and in pregnant individuals bacteria may localize to the placenta inducing premature labor and spontaneous abortion (Blaser et al. 2008; Hoffer 1981).

Many Bacteria and Archaea express a regularly ordered, planar array of identical protein monomers, termed an S layer, on their cell surface (Sleytr and Beveridge 1999). Within the genus *Campylobacter*, only *C. fetus* and *C. rectus* express an S layer and for both species, this outermost cell envelope component is a virulence factor (Blaser et al. 1988; Borinski and Holt 1990). The *C. fetus* S layer undergoes antigenic variation which during relapsing infection in humans (Tu et al. 2005) and in animal models of infection (Garcia et al. 1995; Grogono-Thomas et al. 2000), allows *C. fetus* to escape antibody opsonization and subsequent phagocytic

clearance. In addition, the *C. fetus* S layer provides serum resistance, as it impairs binding of the complement protein C3b (Blaser et al. 1988), and in the absence of opsonizing antibodies, reduces uptake by polymorphonuclear leukocytes (Blaser et al. 1988). In the presence of fibronectin, the S layer also enhances *C. fetus* attachment to eukaryotic cells (Graham et al. 2008).

Metal based compounds have long been appreciated for their antimicrobial activity. Recently, metal oxides of nanoparticle size (particles with an external dimension ranging 1- 100 nm; Lemire et al. 2013) have been found to be particularly toxic at low concentrations to microbes. Zinc oxide nanoparticles display selective toxicity against both gram positive and gram negative bacteria (Jones et al. 2008; Liedtke and Vahjen 2012) as well as against some fungi (Kasemets et al. 2009; Lipovski et al. 2011). Zinc oxide nanoparticle toxicity may be due to destabilization of microbial cell walls and membranes following direct contact with nanoparticles (Brayner et al. 2006; Liu et al. 2009), the release of Zn^{2+} ions (Kasemets et al. 2009; Li et al. 2011), and the generation of reactive oxygen species (ROS) including hydroxyl radicals (•OH), singlet oxygen ($^1O_2$), superoxide anions ($•O_2^-$), and hydrogen peroxide (H_2O_2) (He et al. 2016; Lipovsky et al. 2009; Prasanna and Vijayaraghaven 2015; Sawai et al. 1998). Antimicrobial activity combined with chemical and thermal stability, has led to the incorporation of ZnO nanoparticles into ointments, lotions and surface coatings, including those lining food packaging and storage containers, to control microbial growth (Król et al. 2017; Manna 2012). The objectives of the current study were to determine the susceptibility of *C. fetus* to ZnO nanoparticles and to assess whether the S layer protects *C. fetus* from ZnO nanoparticle damage.

Materials and Methods

Bacterial strains and culture conditions.

Table 1 lists the bacterial strains used in this study. Bacteria were routinely cultured on Columbia agar (Oxoid, Nepean, Ontario) supplemented with 5% (v/v) sheep blood (sBAP; Oxoid) at 37°C for 24 hours under microaerobic conditions (5% O_2: 10% CO_2: 85% N_2). Sheep blood agar supplemented with kanamycin to 50 μg/mL (sBAP/Km) was used for the culture of isogenic S layer deficient strains. *C. jejuni* 81-176 was included as a control organism as its sensitivity to ZnO nanoparticles has been reported (Xie et al. 2011). Cultures were passaged 5 or fewer times for use in all assays. Stock bacterial cultures were stored at -80°C in peptone-glycerol broth (10 g peptone/L, 5 g NaCl/L, 25% (v/v) glycerol).

ZnO nanoparticle antibacterial assays.

Preliminary broth and agar dilution assays ascertained *C. fetus* sensitivity to ZnO nanoparticles. ZnO nanoparticles (30 nm average size, Inframat, Manchester, Connecticut) were suspended in D. H_2O to 100 mg/mL and stored at 4°C (Xie et al. 2011). This stock solution was added to cation adjusted Mueller-Hinton (CA-MH; Oxoid; NCCLS) agar and broth prior to sterilization to generate a range of ZnO nanoparticle concentrations.

(i) Broth dilution assay – kill curve. Minimum inhibitory concentration (MIC) assays assess cell growth visually or spectrophotometrically (i.e., $OD_{600\ nm} < 0.05$; Liedtke and Vahjen 2012). *C. fetus* grows poorly in broth culture, and because ZnO nanoparticles at concentrations exceeding 200 μg/mL themselves contribute to turbidity, MIC assays were not suitable for detecting changes in bacterial growth. As such, a kill curve (Mueller et al. 2004) was used to assess nanoparticle-induced growth inhibition.

Bacteria harvested from solid medium were diluted in CA-MH broth to a concentration of 10^7 CFU/mL as estimated using spectrophotometry ($OD_{600\ nm}$). Viable plate counts ascertained actual bacterial numbers. One hundred μL of the appropriate bacterial strain was

inoculated into 2 mL CA-MH broth, supplemented with kanamycin as required, containing 0, 100, 200, 300 or 500 µg/mL ZnO nanoparticles, and incubated at 37°C under microaerobic conditions with constant shaking (100 rpm). Hourly, for six hours, replicate 100 µL aliquots were removed, serially diluted, and plated on sBAP or for S layer deficient strains, sBAP/Km, to quantify surviving bacteria. After 24 hours exposure to ZnO nanoparticles, a 5 µL aliquot was also spotted onto appropriate agar to assess bacterial cell viability. Assays were repeated three times on separate days.

(ii) Agar dilution assay. Bacteria harvested from solid medium were diluted in CA-MH broth to 10^8 CFU/mL as previously described. Five µL aliquots of each culture were spotted onto CA-MH agar containing 0, 1, 5, 10, 50, or 100 µg/mL ZnO nanoparticles and incubated under a microaerobic atmosphere at 37°C for 96 h at which time bacterial growth was recorded.

(iii) Photoactivation of ZnO nanoparticles: Minimum bacteriocidal concentration and resazurin assay. Minimum bacteriocidal concentration (MBC) values were determined using a microdilution format in 96 well plates. Although aqueous suspensions of ZnO nanoparticles generate ROS including H_2O_2, exposure of ZnO nanoparticle suspensions to ultraviolet or visible light greatly enhances ROS release (Lipovsky et al. 2009; Prasanna and Vijayaraghavan 2015). To determine whether photoactivation would enhance the bacteriocidal activity of ZnO nanoparticles towards *C. fetus*, replicate microdilution assays in 96 well plates were generated; one plate received a 30 min exposure to light, the other plate was not exposed. Full spectrum light was generated using a sodium lamp powered by a Lumatex electronic ballast generating 706 µmoles photons/m^2/sec (LI-250 light meter; Li-Cor Quantum Radiometer Photometer) at the point of contact with the 96 well plate. Duplicate wells received filter sterilized (0.2 µm pore size) catalase (Sigma-Aldrich, Oakville, Ontario) to a final concentration of 4 µg/mL to quench

156 H_2O_2 (Liu et al. 2003). Thus, MBC values were determined under four conditions: CA-MH +
157 ZnO, Dark; CA-MH + ZnO, Light exposure; CA-MH + ZnO + catalase, Dark; and CA-MH +
158 ZnO + catalase, Light exposure.

159 ZnO nanoparticles were serially diluted 2-fold in CA-MH broth. Bacteria were
160 harvested, diluted to 10^7 CFU/mL in CA-MH, and 100 µL volumes were inoculated into each
161 well yielding final concentrations of 2 – 500 µg ZnO nanoparticles/well and 10^6 CFU in a total
162 volume of 200 µL. Control wells contained bacteria either in CA-MH or in CA-MH + catalase
163 (0 µg/mL ZnO).

164 Following inoculation, replicate plates were incubated at 37°C under a microaerobic
165 atmosphere. One plate received a 30 min exposure to light after which incubation was continued
166 in the dark, the other plate was incubated continuously in the dark. After 24 h, the impact of
167 photoactivated ZnO nanoparticles was assessed using both viable plate counts (MBC assay) and
168 resazurin reduction as a measure of metabolic activity. One hundred µL were removed from
169 each well, serially diluted and plated onto sBAP or onto sBAP/Km to enumerate surviving
170 bacteria. Colony counts were collected following 96 h incubation at 37°C in a microaerobic
171 environment. Resazurin (Sigma-Aldrich), also known as Alamar Blue, may be reduced by
172 viable cells to resorufin, a reaction accompanied by a colour change from blue (resazurin) to pink
173 (resorufin). Resazurin was prepared as a stock solution (100 µg/mL) in D. H_2O, filter sterilized
174 and stored in 1 mL aliquots at -20°C. Resazurin was added to the contents remaining in each
175 well to a final concentration of 10 µg/mL. Microtitre plates were incubated in the dark at 37°C
176 under a microaerobic atmosphere for 4 h at which time absorbance was measured at 600 nm
177 (which measures resazurin) and at 570 nm (which measures resorufin) using a Wallac Victor^2

multilabel reader (Fisher Scientific, Mississauga, Ontario). The percent resazurin reduced was calculated using the equation:

$$\frac{[(\varepsilon_{ox}\ \lambda_2)(A\ \lambda_1)]-[(\varepsilon_{ox}\ \lambda_1)(A\ \lambda_2)]}{[(\varepsilon_{red}\ \lambda_1)(A'\ \lambda_2)]-[(\varepsilon_{red}\ \lambda_2)(A'\ \lambda_2)]} \times 100$$

where $\varepsilon_{ox}\ \lambda_2$ = 117,216 (molar extinction coefficient of oxidized resazurin (blue) at 600_{nm}); $\varepsilon_{ox}\ \lambda 1$ = 80,586 (molar extinction coefficient of oxidized resazurin at 570_{nm}); $\varepsilon_{red}\ \lambda_1$ = 155,677 (molar extinction coefficient of reduced resazurin (pink) at 600_{nm}); $\varepsilon_{red}\ \lambda_2$ = 14,652 (molar extinction coefficient of reduced resazurin at 570_{nm}); $A\ \lambda_1$ is the absorbance at 570_{nm} of the experimental samples; $A\ \lambda_2$ is the absorbance at 600_{nm} of the experimental samples; $A'\ \lambda_1$ is the absorbance at 570_{nm} of the control samples which contained CA-MH ± ZnO ± catalase but which were not inoculated with bacteria; A' λ2 is the absorbance at 600_{nm} of these control samples (McBride et al. 2005; Pettit et al. 2005). Inhibition of metabolic activity was defined as ≤ 50% resazurin reduction (Pettit et al. 2005). Microdilution assays for MBC and resazurin reduction were repeated at least twice on separate days.

Transmission electron microscopy. Samples of ZnO nanoparticles were diluted in D. H_2O to 100 µg/mL, deposited onto formvar coated, carbon backed 200 mesh copper grids and observed unstained in a Phillips EM410 transmission electron microscope at an operating voltage of 80 KeV.

To visualize the impact of ZnO nanoparticles on *C. fetus* cell morphology, 10^9 CFU/mL bacteria were exposed to 500 µg/mL ZnO for 4 h at 37°C. Nanoparticles were removed by washing in 0.05 M HEPES (N-2-hydroxyethylpiperazine-N'-2-ethanesulfonic acid; Research Organics) buffer, pH 6.8, and pelleted cells were enrobed in 2% Noble agar. Bacteria were fixed in HEPES buffer containing 2% glutaraldehyde and 2.5% p-formaldehyde and processed for thin section transmission electron microscopy as described (Graham and Beveridge 1990).

Campylobacter fetus was also processed using freeze-substitution in 2% osmium tetroxide and 2% uranyl acetate in anhydrous acetone as described (Graham and Beveridge 1990). Thin sections were stained with 2% uranyl acetate and Reynolds lead citrate prior to viewing.

Statistical analysis. Differences in bacterial cell survival between S layer expressing and S layer deficient *C. fetus* strains were assessed using a multi-way analysis of variance (ANOVA) with a post-hoc Bonferoni test followed by a pair-wise comparison of sample means. Pooled bacterial count data were not normally distributed as determined using a one sample Kolmogorov-Smirnov test. As such, data were log transformed prior to ANOVA analysis. Statistical significance was assessed at a $\rho \leq 0.05$. Statistical analysis was performed using Systat 7.1.0 (SPSS Inc., Chicago, IL).

RESULTS

ZnO nanoparticles are bacteriocidal for *C. fetus*.

Transmission electron microscopy of commercially acquired ZnO nanoparticles revealed a range of particle size and morphology (Fig. 1). Despite this variation, kill curves indicated a concentration dependent decrease in cell viability for all bacterial strains assessed during a 6 h exposure to ZnO nanoparticles (Fig. 2). After 24 h exposure, no viable bacteria were recovered, indicating that ZnO nanoparticles are bacteriocidal for *C. fetus* and *C. jejuni*. In contrast, control bacteria incubated in the absence of ZnO nanoparticles remained viable throughout the assay and were recovered at 24 h. No difference ($\rho \geq 0.05$) in bacterial cell viability was noted between wild type and corresponding isogenic S layer deficient *C. fetus* strain at any nanoparticle concentration. In agar dilution assays, *C. fetus* growth was observed at ZnO nanoparticle concentrations of 0 – 50 μg/mL; no growth was observed for any *C. fetus* strain inoculated onto

CA-MH agar containing 100 µg/mL ZnO (data not shown). *C. jejuni* growth was inhibited at 50 and 100 µg/mL ZnO. Together, these results indicate that ZnO nanoparticles are bacteriocidal for *C. fetus*.

The antibacterial activity observed in both broth and agar dilution assays was reflected in the morphology of *C. fetus* cells exposed to nanoparticles. Transmission electron microscopy showed zinc oxide-exposed cells with altered envelope morphology including variable distance between plasma and outer membranes, increased membrane waviness and gaps in cytoplasmic contents (Fig. 3). In contrast, unexposed control cells displayed smooth envelope profiles and evenly distributed cytoplasmic contents.

Photoactivation enhances ZnO nanoparticle activity towards *C. fetus*.

To determine whether photoactivation would increase the bacteriocidal activity of ZnO nanoparticles towards *C. fetus*, MBC assays were performed in duplicate 96 well plates in which one plate received a 30 minute light exposure while the replicate plate was incubated continuously in the dark (Fig. 4). MBC values ≥125 µg/mL were observed for all *C. fetus* strains incubated with ZnO nanoparticles in the dark. When cells received a 30 minute light exposure, MBC values decreased to 16 – 62.5 µg/mL. Catalase enhanced bacterial resistance to photoactivated ZnO nanoparticles, in some cases restoring MBC levels to those observed in dark incubated cells, indicating that H_2O_2 generation contributes to *C. fetus* cell death. For bacteria incubated with ZnO nanoparticles in the dark, the presence or absence of catalase had no impact on MBC values. Interestingly, MBC values were lower for S layer deficient *C. fetus* strains than for wild type S layer expressing strains when cells were incubated with photoactivated zinc oxide nanoparticles. In contrast, neither photoactivation nor the presence of catalase impacted the recovery of *C. jejuni* exposed to ZnO nanoparticles. These data indicate that light enhances the

antibacterial activity of ZnO nanoparticles towards *C. fetus* and that the S layer imparts resistance to this antibacterial activity.

Some bacteria including *C. jejuni*, may exist in a viable but non-culturable (VBNC) state in which metabolic activity is detectable despite an absence of cell growth (Li et al. 2014; Portner et al. 2007; Zhao et al. 2017). To exclude the possibility that *C. fetus* remained viable despite the absence of colony growth on agar, *C. fetus* cells exposed to ZnO nanoparticles for 24 h were also assessed for their ability to reduce resazurin as an indicator of cell metabolism (Fig. 5). Resazurin reduction results mirrored MBC assays – when no viable bacteria were recovered in plating assays, resazurin reduction was ≤ 50% (metabolic activity was defined as resazurin reduction levels of ≥ 50%; Pettit et al. 2005). *C. fetus* retained the ability to reduce resazurin in the presence of greater ZnO nanoparticle concentrations when bacteria were incubated in the dark compared to cells receiving a 30 minute light exposure. As observed in MBC assays, the presence of catalase did not impact resazurin reduction for dark incubated cells but did ameliorate the inhibition observed in light exposed cells (Fig. 5, compare Light versus Light + cat). For *C. jejuni*, percent resazurin reduction was only impacted by ZnO nanoparticle concentration, neither light exposure nor catalase altered the levels of resazurin reduction.

Discussion

As the outermost component of the prokaryotic cell envelope, S layers are uniquely positioned to interface between the cell and its immediate environment. S layers have been shown to protect against a number of environmental threats including *Bdellovibrio bacteriovorus* predation (Koval 1993; Koval and Hynes 1991), bacteriophage (Ishiguro et al. 1981), the bacteriocidal action of complement proteins (Blaser et al. 1988; Munn et al. 1982), and recently cationic antimicrobial peptides (de la Fuente-Núñez et al. 2012). Here, we compared the impact

of ZnO nanoparticles on wild type S layer expressing and isogenic S layer deficient mutants and show that not only is *C. fetus* sensitive to these nanoparticles, but also that the *C. fetus* S layer provides protection from H_2O_2 generated during photoactivation of ZnO nanoparticles.

Zinc oxide nanoparticles of various shape and size exhibit antimicrobial activity against a broad range of gram positive and negative bacteria (reviewed in Kumar et al. 2017). Kill curves and agar dilution assays reveal that ZnO nanoparticles at 100 µg/mL are bacteriocidal for *C. fetus* as control bacteria cultured in the absence of nanoparticles remained viable. The dose dependent reduction in cell viability observed here for *C. fetus* exposed to ZnO nanoparticles, has been reported for other *Campylobacter* species, including *C. jejuni* (Xie et al. 2011) and *C. coli* (Bratz et al. 2013). For *C. jejuni*, MIC values range from 25 – 290 µg/mL ZnO nanoparticles as a function of strain (Liedtke and Vahjemn 2012; Xie et al. 2011). And although *C. jejuni* cultured as a biofilm was more resistant to ZnO nanoparticles than were planktonic cells, ZnO nanoparticles were bacteriocidal following a 10 h exposure at 1.2 mmol (100 µg/mL), regardless of growth format (Lu et al. 2012). Growth of *C. coli* 5981 was significantly reduced after 24 h exposure to 200 µg/mL ZnO powder, though some cells remained viable at 24 h in the presence of 500 µg/mL ZnO (Bratz et al. 2013). Other enteric gram negative bacteria, including *E. coli* O157:H7, have MIC values of at least 400 µg/mL ZnO nanoparticles (Xie et al. 2011) and like *C. coli*, some cells may even remain viable at these concentrations (Liu et al. 2009).

C. fetus sensitivity to ZnO nanoparticles was reflected in changes in cell morphology. TEM of ZnO exposed *C. fetus* revealed spiral shaped cells with enlarged periplasm and wavy membranes. Exposure of *C. jejuni* to 500 µg/mL ZnO nanoparticles for 12 h resulted in a change from spiral to coccal morphology, a form associated with a VBNC state (Xie et al. 2011). No switch to the coccal form was observed for *C. fetus*. Levels of resazurin reduction were

295 correlated with the killing observed in MBC assays. Thus, we found no evidence to suggest that
296 ZnO nanoparticles induce a VBNC state in *C. fetus*, rather, ZnO nanoparticles are bacteriocidal
297 for *C. fetus*.

298 The antibacterial activity of ZnO nanoparticles has been linked to disruption of cell
299 membranes (Xie et al. 2011), toxicity due to the release of Zn^{2+} ions (Pasquet et al. 2014) and the
300 production of ROS. Any of these mechanisms could be responsible for the bacteriocidal activity
301 observed when *C. fetus* was incubated with ZnO nanoparticles in the dark. Aqueous
302 suspensions of ZnO nanoparticles incubated in the dark generate hydroxyl radicals ($OH^{\bullet}$) (He et
303 al. 2016; Lipovsky et al. 2009) as well as superoxide ($\bullet O^{2-}$) and H_2O_2 (Prasanna and
304 Vijayaraghavan 2015; Sawai et al. 1998). Exposure of aqueous ZnO suspensions to UV or
305 visible light increases production of these ROS (Lipovsky et al. 2009; Prasanna and
306 Vijayaraghavan 2015). In the current study, photoactivation dramatically enhanced the
307 bacteriocidal activity of ZnO nanoparticles. For all *C. fetus* strains, MBC values were lowest
308 when bacteria were incubated with ZnO nanoparticles and had been exposed to light. The
309 addition of catalase reduced this light enhanced killing effect, suggesting that H_2O_2 is a major
310 contributor to *C. fetus* cell death. Though H_2O_2 is not as reactive as the other ROS (Blake et al.
311 1999), H_2O_2 can oxidize unsaturated phospholipids in cell membranes, thereby decreasingly
312 membrane fluidity and altering membrane properties (Cabiscol et al. 2000; Sawai et al. 1998).
313 And if intracellular, in the presence of metal ions such as Fe^{2+} and Mn^{2+}, H_2O_2 is readily
314 converted to highly reactive •OH via the Fenton reaction (Lemire et al. 2013). In response to
315 ZnO nanoparticle exposure, both *C. jejuni* and *C. coli* have demonstrated up regulation of stress
316 response genes including *katA* (which encodes catalase, an enzyme which degrades H_2O_2)
317 implying a role for ROS, specifically H_2O_2, in cell killing (Bratz et al. 2013; Xie et al. 2011). *C.*

318 *jejuni* lacks an S layer and was hypothesized to react to ZnO nanoparticles in a manner similar to
319 S layer deficient *C. fetus* strains. In our hands, however, photoactivation did not enhance ZnO
320 nanoparticle action against *C. jejuni*, nor did the presence of catalase ameliorate cell death,
321 suggesting that unlike *C. fetus*, H_2O_2 may not be a major contributor to ZnO nanoparticle
322 induced *C. jejuni* cell death.

323 Given the variation in size and shape of the commercially acquired ZnO nanoparticles, it
324 is not possible to state that the *C. fetus* S layer physically excluded nanoparticles from directly
325 interacting with cell membranes. And for bacteria exposed to ZnO nanoparticles in the dark we
326 did not observe any difference in susceptibility between S layer expressing and S layer deficient
327 *C. fetus* strains. S layer expressing strains were however, found to be more resistant to
328 photoactivated ZnO nanoparticles than were S layer deficient *C. fetus* strains. Arrangement of
329 protein monomers into a lattice array with regularly spaced pores of defined size, enables S
330 layers to function as permeability barriers, filtering according to size and even charge (Beveridge
331 and Graham 1991). Charge interactions between negatively charged amino acids in the
332 *Caulobacter crescentus* S layer and positively charged cationic antimicrobial peptides were
333 proposed to prevent the peptides from reaching the bacterial outer membrane, thereby protecting
334 *C. crescentus* cells (de la Fuente-Núñez, et al. 2012). Although all of the ROS generated from
335 ZnO nanoparticles would be S layer permeable based upon size, the net negative charge of the *C.*
336 *fetus* S layer (Blaser and Gotschlich 1990) would likely repel negatively charged hydroxyl
337 radicals and superoxide anions. Hydrogen peroxide in contrast, is uncharged and could readily
338 traverse the S layer. For *C. fetus* VC119, S layer subunits were estimated to be 11 nm in height
339 (Dubreiul et al. 1990) and would thus position the S layer away from the underlying cell surface.
340 In *C. fetus* 809, the S layer is also visible external to the underlying outer membrane (Fig. 3A).

The distance between S layer and outer membrane may be significant. When ZnO nanoparticles interact with the S layer, H_2O_2 generated may oxidize S layer protein monomers directly or LPS polymers residing beneath the S layer, essentially quenching H_2O_2 reactivity. These "off-target" reactions would reduce the amount of H_2O_2 accessing cell membranes and cytoplasm. In the absence of the S layer, nanoparticles themselves could penetrate deeper into the cell envelope, i.e., to the outer membrane surface, and the ROS generated in closer proximity to cell membranes could incur more cell damage. As ROS including H_2O_2 are produced in greater concentrations during light exposure (Manna 2012), the S layer barrier effect is more apparent in light exposed than in dark incubated bacteria. At elevated ZnO nanoparticle concentrations (i.e., > 100 μg/mL), damage due to ROS or other killing mechanisms would be extensive and likely exceed quenching capacity thus negating the benefit of S layer expression. Other cell envelope layers including capsules exhibit similar barrier qualities. The extracellular polymeric substance expressed on *Rothia mucilaginosa* Ora-16, an emerging opportunistic oral pathogen, protected these cells from killing with ZnO nanoparticles compared to cells lacking this envelope layer (Khan et al. 2014). Similarly, exopolysaccharides protected *Bacillus subtilis* from ZnO nanoparticle toxicity (Hsueh et al. 2015). *C. jejuni* 81-176 also expresses capsular polysaccharide (Bacon et al. 2001) and this envelope component may have protected cells from the impact of photoactivation in the current study.

Although the difference in MBC values for *C. fetus* exposed to photoactivated ZnO nanoparticles in the presence and absence of catalase implicates H_2O_2 in cell killing, this does not preclude killing via the other proposed mechanisms of ZnO activity, including Zn^{2+} ion toxicity. Although not addressed in the current study, free Zn^{2+} ions may bind acidic amino acids in the *C. fetus* S layer (Blaser and Gotschlich 1990) or displace the divalent cations which

mediate *C. fetus* S layer attachment to underlying LPS (Yang et al. 1992). Either binding mechanism would reduce the amount of free Zn^{2+} reaching the cytoplasm, thereby reducing toxicity. Though at elevated ZnO nanoparticle concentrations (i.e., >100 μg/mL) free Zn^{2+} ions would saturate the cell surface and any protective benefit provided by the S layer would be lost.

In conclusion, we have shown that zinc oxide nanoparticles are bacteriocidal for *C. fetus* and that this antibacterial activity is greatly enhanced following photoactivation. Hydrogen peroxide contributes to the bacteriocidal activity generated during photoactivation. S layer expressing strains are more resistant to this H_2O_2 mediated killing than are S layer deficient strains indicating a protective role for this cell envelope component. As the interface between the bacterial cell and its environment, the S layer is ideally positioned to provide this barrier function.

Acknowledgements

We wish to acknowledge the StFX University Council for Research and the Dr. Leo P. Chaisson Research Endowment for financial support (SEF). We also acknowledge the StFX University Microscopy Facility and technical assistance from Dr. G. Robertson.

References

Bacon, D.J., Szymanski, C.M., Burr, D.H., Silver, R.P., Alm, R.A., and Guerry, P. 2001. A phase-variable capsule is involved in virulence of *Campylobacter jejuni* 81-176. Molecular Microbiology, **40:** 769-777.

Beveridge, T.J., and Graham, L.L. 1991. Surface layers of bacteria. Microbiology Reviews, **55**(4): 684 – 705.

Blaser, M.J., and Gotschlich, E.C. 1990. Surface array protein of *Campylobacter fetus*. The Journal of Biological Chemistry, **265**(24): 14529 – 14535.

Blaser, M.J., Newell, D.N., Thompson, S.A., and Zechner, E.L. 2008. Pathogenesis of *Campylobacter fetus*. *In Campylobacter*, 3rd ed. *Edited by* I. Nachamkin, C.M. Zymanski, and M.J. Blaser. ASM Press, Washington, D.C. pp. 401-428.

Blaser, M.J., Smith, P.F., Repine, J.E., and Joiner, K.A. 1988. Pathogenesis of *Campylobacter fetus* infections. Failure of encapsulated *Campylobacter fetus* to bind C3b explains serum and phagocytosis resistance. The Journal of Clinical Investigation, **81:** 1434 – 1444.

Blake, D.M., Maness, P.-C., Huang, Z., Wolfrum, E.J., Huang, J., and Jacoby, W.J. 1999. Application of the photocatalytic chemistry of titanium dioxide to disinfection and the killing of cancer cells. Separation and Purification Reviews, **28**(1): 1-50.

Borinski, R., and Holt, S.C. 1990. Surface characteristics of *Wolinella recta* ATCC 33238 and human clinical isolates: correlation of structure with function. Infection and Immunity, **58**(9): 2770 – 2776.

Bratz, K., Gölz, G., Riedel, C., Janczyk, P., Nöckler, K., and Alter, T. 2013. Inhibitory effect of high-dosage zinc oxide dietary supplementation on *Campylobacter coli* excretion in weaned piglets. Journal of Applied Microbiology, **115**: 1194-1202.

Brayner, R., Ferrari-Iliou, R., Brivois, N., Djediat, S., Benedetti, M.F., and Fievet, F. 2006. Toxicological impact studies based on *Escherichia coli* bacteria in ultrafine ZnO nanoparticles colloidal medium. Nano Letters, **6:** 866 – 870.

Cabiscol, E., Tamarit, J., and Ros, J. 2000. Oxidative stress in bacteria and protein damage by reactive oxygen species. International Microbiology, **3**: 3 – 8.

Dubrueil, J.D., Kostrzynska, M., Austin, J.W., and Trust, T.J. 1990. Antigenic differences among *Campylobacter fetus* S-Layer proteins. Journal of Bacteriology, **172**(9): 5035 – 5043.

de la Fuente-Núñez, C., Mertens, J., Smit, J., and Hancock, R.E.W. 2012. The bacterial surface layer provides protection against antimicrobial peptides. Applied and Environmental Microbiology, **78**(8): 5452-5456.

Garcia, M.M., Lutze-Wallace, C.L., Denes, A.S., Eaglesome, M.D., Holst, E., and Blaser, M.J. 1995. Protein shift and antigenic variation in the S-layer of *Campylobacter fetus* subsp. *venerealis* during bovine infection accompanied by genomic rearrangement of *sapA* homologs. Journal of Bacteriology, **177**(8): 1976-1980.

Gilbert, M.J., Kik, M., Timmerman, A.J., Severs, T.T., Kusters, J.G., Duim, B., and Wagenaar, J.A. 2014. Occurrence, diversity and host association of intestinal *Campylobacter*,

427 *Arcobacter*, and *Helicobacter* in reptiles. PLoS One **9**: e101599. doi:
428 10.1371/journal.pone.0101599 PMID: 24988130.

429 Graham, L.L., and Beveridge, T.J. 1990. Evaluation of freeze-substitution and conventional
430 embedding protocols for routine electron microscopic processing of eubacteria. Journal
431 of Bacteriology, **172**(4): 2141-2149.

432 Graham, L.L., and MacDonald, K.L. 1998. The *Campylobacter fetus* S layer is not essential for
433 initial interaction with HEp-2 cells. Canadian Journal of Microbiology, **44:** 244 – 250.

434 Graham, L.L., Friel, T., and Woodman, R.L. 2008. Fibronectin enhances *Campylobacter fetus*
435 interaction with extracellular matrix components and INT 407 cells. Canadian Journal of
436 Microbiology, **54**: 37 – 47.

437 Grogono-Thomas, R., Dworkin, J., Blaser, M.J., and Newell, D.G. 2000. Roles of the surface
438 layer proteins of *Campylobacter fetus* subsp. *fetus* in ovine abortion. Infection and
439 Immunity, **68**(3): 1687-1691.

440 He, W., Jia, H., Cai, J., Han, X., Zheng, Z., Wamer, W.G., and Yin, J.-J. 2016. Production of
441 reactive oxygen species and electrons from photoexcited ZnO and ZnS nanoparticles: A
442 comparative study for unraveling their distinct photocatalytic activities. The Journal of
443 Physical Chemistry C, **120**: 3187-3195. doi: 10.1201/acs.jpcc.5b11456.

444 Hoffer, M.A. 1981. Bovine Campylobacteriosis: A review. Canadian Veterinary Journal, **22**:
445 327-330.

446 Hsueh, Y.-H., Ke, W.-J., Hsieh, C.-T., Lin, K.-S., Tzou, D.-Y., and Chiang, C.-L. 2015. ZnO
447 nanoparticles affect *Bacillus subtilis* cell growth and biofilm formation. PLoS One, **10**:
448 e0128457. doi: 10.1371/journal.pone.0128457.

449 Ishiguro, E.E., Kay, W.W., Ainsworth, T., Chamberlain, J. B., Austen, R.A., Buckley, J.T., and
450 Trust, T.J. 1981. Loss of virulence during culture of *Aeromonas salmonicida* at high
451 temperature. Journal of Bacteriology, **148**(1): 333 – 340.

452 Jones, N., Ray, B., Ranjit, K.T., and Manna, A.C. 2008. Antibacterial activity of ZnO
453 nanoparticle suspensions on a broad spectrum of microoorganisms. FEMS Microbiology
454 Letters, **279:** 71 – 76.

455 Kaakoush, N.O., Castaño-Rodriguez, N., Mitchell, H.M., and Man, S.M. 2015. Global
456 epidemiology of *Campylobacter* infection. Clinical Microbiology Reviews, **28**: 687-
457 720. doi:10.128/CMR.00006-15.

458 Kasemets, K., Ivask, A., Dubourguier, H.-C., and Kahru, A. 2009. Toxicity of nanoparticles of
459 ZnO, CuO and TiO_2 to yeast *Saccharomyces cerevisiae.* Toxicology In Vitro, **23**: 1116
460 – 1122.

461 Khan, S.T., Ahamed, M., Musarrat, J., and Al-Khedhairy, A.A. 2014. Anti-biofilm and
462 antibacterial activities of zinc oxide nanoparticles against the oral opportunistic
463 pathogens *Rothia dentocariosa* and *Rothia mucilaginosa*. European Journal of Oral
464 Sciences, **122**: 397-403. doi: 10.1111/eos.12152.

465 Kienesberger, S., Sprenger, H., Wolfgruber, S., Halwachs, B., Thallinger, G.G., Perez-Perez,
466 G.I., Blaser, M.J., and Zechner, E.L. 2014. Comparative genome analysis of
467 *Campylobacter fetus* subspecies revealed horizontally acquired genetic elements

important for virulence and niche specificity. PLoS One, **9**: e85491. doi: 10.1371/journal.pone.0085491.

Koval, S.F. 1993. Predation on bacteria possessing S-layers. *In* Advances in Paracrystalline Bacterial Surface Layers. *Edited by* T.J. Beveridge and S.F. Koval. Plenum Press, New York. pp. 85-92.

Koval, S.F., and Hynes, S.H. 1991. Effect of paracrystalline protein surface layers on predation by *Bdellovibrio bacteriovorus*. Journal of Bacteriology, **173**(7): 2244-2249.

Król, A., Pomastowski, P., Rafińska, K., Railean-Plugaru, V., and Buszewski, B. 2017. Zinc oxide nanoparticles: Synthesis, antiseptic activity and toxicity mechanism. Advances in Colloid and Interface Science, **249**: 37-52.

Kumar, R., Umar, A., Kumar, G., and Nalwa, H.S. 2017. Antimicrobial properties of ZnO nanomaterials. A review. Ceramics International, **43**: 3940-3961.

Lemire, J.A., Harrison, J.J., and Turner, R.J. 2013. Antimicrobial activity of metals: mechanisms, molecular targets and applications. Nature Reviews Microbiology, **11**: 371-384.

Li, L., Mendis, N., Trigui, H., Oliver, J.D., and Faucher, S.P. 2014. The importance of the viable but non-culturable state in human bacterial pathogens. Frontiers in Microbiology, **5**: 258. doi: 10.3389/fmicb.2014.00258.

Li, M., Zhu, L., and Lin, D. 2011. Toxicity of ZnO nanoparticles to *Escherichia coli*: mechanism and the influence of medium components. Environmental Science and Technology, **45:** 1977 – 1983.

Liedtke, J., and Vahjen, W. 2012. In vitro antibacterial activity of zinc oxide on a broad range of reference strains of intestinal origin. Veterinary Microbiology, **160:** 251 – 255.

Lipovsky, A., Nitzan, Y., Gedanken, A., and Lubart, R. 2011. Antifungal activity of ZnO nanoparticles- the role of ROS mediated cell injury. Nanotechnology, **22**: 105101. doi: 10.1088/0957-4484/22/10/105101.

Lipovsky, A., Tzitrinovich, Z., Friedmann, H., Applerot, G., Gedanken, A., and Lubart, R. 2009. EPR study of visible light-induced RPS generation by nanoparticles of ZnO. Journal of Physical Chemistry C, **113:** 15997 – 16001.

Liu, W., Andrews, S.A., Stefan, M.I., and Bolton, J.R. 2003. Optimal methods for quenching H_2O_2 residuals prior to UFC testing. Water Research, **37:** 3697-3703.

Liu, Y., He, L., Mustapha, A., Li, H., Hu, Z.Q., and Lin, M. 2009. Antibacterial activities of zinc oxide nanoparticles against *Escherichia coli* O157:H7. Journal of Applied Microbiology, **107:** 1193 – 1201.

Lu, X., Weakley, A.T., Aston, D.E., Rasco, B.A., Wang, S., and Konkel, M.E. 2012. Examination of nanoparticle inactivation of *Campylobacter jejuni* biofilms using infrared and Raman spectroscopies. Journal of Applied Microbiology, **113:** 952-963. doi: 10.1111/j.1365-2672.2012.05373.x.

Manna, A.C. 2012. Synthesis, characterization and antimicrobial activity of zinc oxide nanoparticles. *In* Nano-antimicrobials: Progress and Prospects. *Edited by* N. Cioffi and M. Ra. Springer, New York, NY. pp. 151-180.

McBride, J., Ingram, P.R., Henriquez, F.L., and Roberts, C.W. 2005. Development of colorimetric microtiter plate assay for assessment of antimicrobials against *Acanthamoeba*. Journal of Clinical Microbiology, **43**(2): 629 – 634.

512 Mueller, M., de al Peña, A., and Derendorf, H. 2004. Issues in pharmacokinetics and
513 pharmacodynamics of anti-infective agents: Kill curves versus MIC. Antimicrobial
514 Agents and Chemotherapy, **48**(2): 369-377. doi: 10.1128/AAC.48.2.369-377.2004
515 Munn, C.B., Ishiguro, E.E., Kay, W.W., and Trust, T.J. 1982. Role of surface components in
516 serum resistance of virulent *Aeromonas salmonicida*. Infection and Immunity, **36**(3):
517 1069 – 1075.
518 NCCLS, National Committee on Clinical Laboratory Standards. 2003. Methods for Dilution
519 Antimicrobial Susceptibility Tests for Bacteria That Grow Aerobically; Approved
520 Standard. 6th ed. NCCLS doc. M7-A6.
521 Pasquet, J., Chevalier, Y., Pelletier, J., Couval, E., Bouvier, D., and Bolzinger, M.-A. 2014.
522 The contribution of zinc ions to the antimicrobial activity of zinc oxide. Colloids and
523 Surfaces A: Physicochemical and Engineering Aspects, **457**: 263-274.
524 Pettit, R.K., Weber, C.A., Kean, M.J., Hoffmann, H., Pettit, G.R., Tan, R., Franks, K.S., and
525 Horton, M.L. 2005. Microplate Alamar Blue assay for *Staphylococcus epidermidis*
526 biofilm susceptibility testing. Antimicrobial Agents and Chemotherapy, **49**(7): 2612-
527 2617.
528 Portner, D.C., Leuschner, R.G., and Murray, S.S. 2007. Optimising the viability during storage
529 of freeze-dried cell preparations of *Campylobacter jejuni*. Cryobiology, **54**: 265-270.
530 Prasanna, V.L., and Vijayaraghaven, R. 2015. Insight into the mechanisms of antibacterial
531 activity of ZnO: Surface defects mediated reactive oxygen species even in the dark.
532 Langmuir, **l31**: 9155-9162. doi: 10.1021/acs.langmuir.5b02266.

533 Sawai, J., Shoji, S., Igarashi, H., Hashimoto, A., Kokugan, T., Shimizu, M., and Kojima, H.
534 1998. Hyrdogen peroxide as an antibacterial factor in zinc oxide powder slurry. Journal
535 of Fermentation and Bioengineering, **86**(5): 521 – 522.
536 Sleytr, U.B., and Beveridge, T. J. 1999. Trends in Microbiology, **7**: 253-260.
537 Tu, Z.-C., Gaudreau, C., and Blaser, M.J. 2005. Mechanisms underlying *Campylobacter fetus*
538 pathogenesis in humans: Surface-layer protein variation in relapsing infections. Journal
539 of Infectious Diseases, **191**: 2082-2089.
540 Xie, Y., He, Y., Irwin, P.L., Jin, T., and Shi, X. 2011. Antibacterial activity and mechanism of
541 action of zinc oxide nanoparticles against *Campylobacter jejuni*. Applied and
542 Environmental Microbiology, **77**(7): 2325 – 2331.
543 Yang, L., Pei, Z., Fujimoto, S., and Blaser, M.J. 1992. Reattachment of surface array proteins to
544 *Campylobacter fetus* cells. Journal of Bacteriology, **174**(4): 1258-1267.
545 Zhao, X., Zhong, J., Wei, C., Lin, C.-W., and Ding, T. 2017. Current perspectives on viable but
546 non-culturable state in foodborne pathogens. Frontiers in Microbiology, **8:** 580. doi:
547 10.3389/fmicb.2017.00580.

Figure legends

Figure 1. Unstained, whole mount of zinc oxide nanoparticles observed using transmission electron microscopy. Bar represents 500 nm.

Figure 2. Impact of zinc oxide nanoparticles on *C. fetus*. Bacteria were incubated with ZnO nanoparticles and bacterial survival determined hourly using viable plate counts. Data is shown as the mean + SD of 3 separate experiments performed on different days. No difference ($\rho \geq 0.05$) in bacterial survival was noted between wild type and corresponding S layer deficient *C. fetus* strain at any nanoparticle concentration. **Cff**, *Campylobacter fetus* subsp. *fetus*; **Cfv**, *Campylobacter fetus* subsp. *venerealis*. **Cj**, *Campylobacter jejuni*. S layer deficient strains are indicated by the letter "K" following the strain number.

Figure 3. Thin section transmission electron micrographs of *C. fetus*. (**A**) Freeze-substituted *C. fetus* 809. Arrow indicates the S layer. Bar represents 100 nm. (**B**) *C. fetus* 13783 incubated in the absence of ZnO nanoparticles and processed by conventional fixation. Bar represents 500 nm. (**C**) *C. fetus* 13783 exposed to 500 μg/mL ZnO nanoparticles for 4 h in the dark and processed by conventional fixation. Bar represents 500 nm.

Figure 4. Photoactivation enhances ZnO nanoparticle activity towards *C. fetus*. MBC assays were conducted in duplicate 96 well plates incubated at 37℃ under microaerobic conditions. Following bacterial inoculation, one plate was incubated in the dark (**Dark**) and the duplicate plate was exposed to visible light for 30 min (**Light**) prior to incubation in the dark. Catalase (4 μg/mL) was included in replicate wells (**Dark + catalase**; **Light + catalase**). After 24 h exposure to ZnO nanoparticles, surviving bacteria were enumerated using viable plate counts. Data is presented as the mean +

572 SD of at least 2 independent assays conducted on different days. **Cff**, *C. fetus* subsp.
573 *fetus*; **Cfv**, *C. fetus* subsp. *venerealis*; **Cj**, *C. jejuni*. S layer deficient strains are
574 indicated by the letter "K" following the strain number.

575 Figure 5. Zinc oxide nanoparticles inhibit bacterial metabolic activity. Resazurin reduction, an
576 indicator of cell metabolic activity, was assessed after 24 h exposure to ZnO
577 nanoparticles. Data shown is representative of 2 replicate assays. Dark bars indicate
578 loss of metabolic activity (≤ 50% resazurin reduction). Grey bars indicate residual
579 metabolic activity.

580

581

Table 1. Bacterial strains used in this study.

Species, strain	Relevant Characteristics	Source or Reference
Campylobacter fetus subsp. *fetus*		
13783	Human blood isolate; S layer expressing	F. Rogers, NML*, Winnipeg, Canada
11686	Human blood isolate; S layer expressing	F. Rogers, NML, Winnipeg, Canada
13783K	S layer deficient *C. fetus* 13783, Km^r †	Graham et al., 2008
11686K	S layer deficient *C. fetus* 11686, Km^r	Graham et al., 2008
Campylobacter fetus subsp. *venerealis*		
809	Human blood isolate; S layer expressing	D.E. Taylor, U. Alberta, Edmonton, Canada
809K	S layer deficient *C. fetus* 809, Km^r	Graham and MacDonald, 1998
Campylobacter jejuni subsp. *jejuni*		
81-176	Human diarrhea isolate	B.B. Finlay, U. British Columbia, Vancouver, Canada

*NML, National Microbiology Laboratory
†Km^r, kanamycin resistant

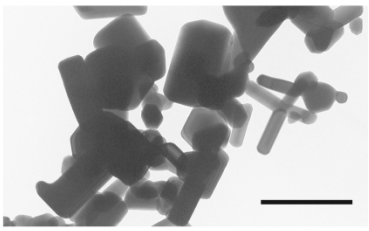

Figure 1. Unstained, whole mount of zinc oxide nanoparticles observed using transmission electron microscopy. Bar represents 500 nm.

215x279mm (300 x 300 DPI)

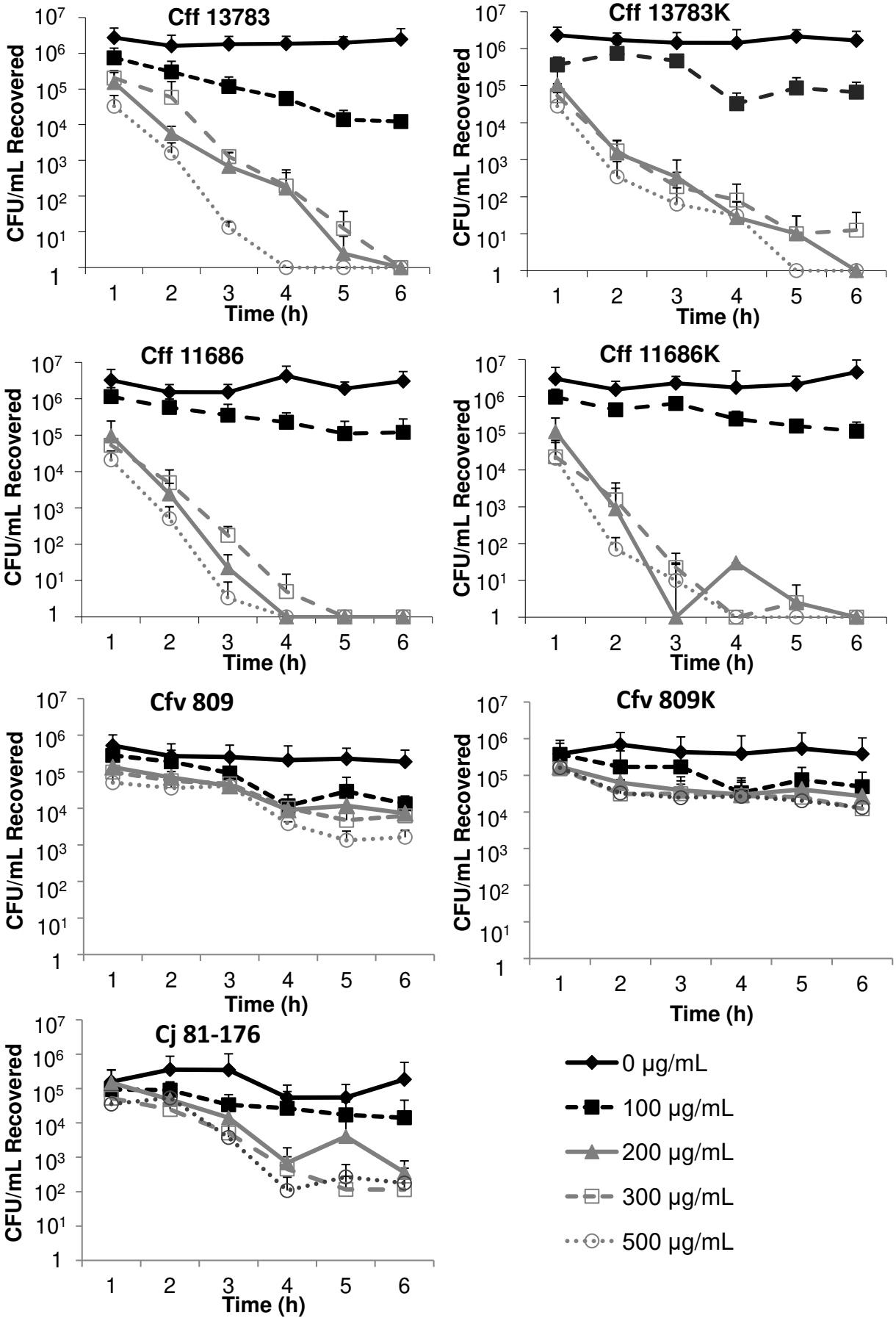
Cff 13783
Cff 13783K
Cff 11686
Cff 11686K
Cfv 809
Cfv 809K
Cj 81-176
CFU/mL Recovered
Time (h)
0 µg/mL
100 µg/mL
200 µg/mL
300 µg/mL
500 µg/mL

Figure 2. Impact of zinc oxide nanoparticles on C. fetus. Bacteria were incubated with ZnO nanoparticles and bacterial survival determined hourly using viable plate counts. Data is shown as the mean + SD of 3 separate experiments performed on different days. No difference ($\rho \geq 0.05$) in bacterial survival was noted between wild type and corresponding S layer deficient C. fetus strain at any nanoparticle concentration. Cff, Campylobacter fetus subsp. fetus; Cfv, Campylobacter fetus subsp. venerealis. Cj, Campylobacter jejuni. S layer deficient strains are indicated by the letter "K" following the strain number.

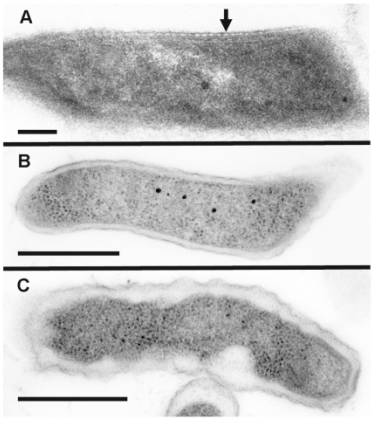

Figure 3. Thin section transmission electron micrographs of C. fetus. (A) Freeze-substituted C. fetus 809. Arrow indicates the S layer. Bar represents 100 nm. (B) C. fetus 13783 incubated in the absence of ZnO nanoparticles and processed by conventional fixation. Bar represents 500 nm. (C) C. fetus 13783 exposed to 500 µg/mL ZnO nanoparticles for 4 h in the dark and processed by conventional fixation. Bar represents 500 nm.

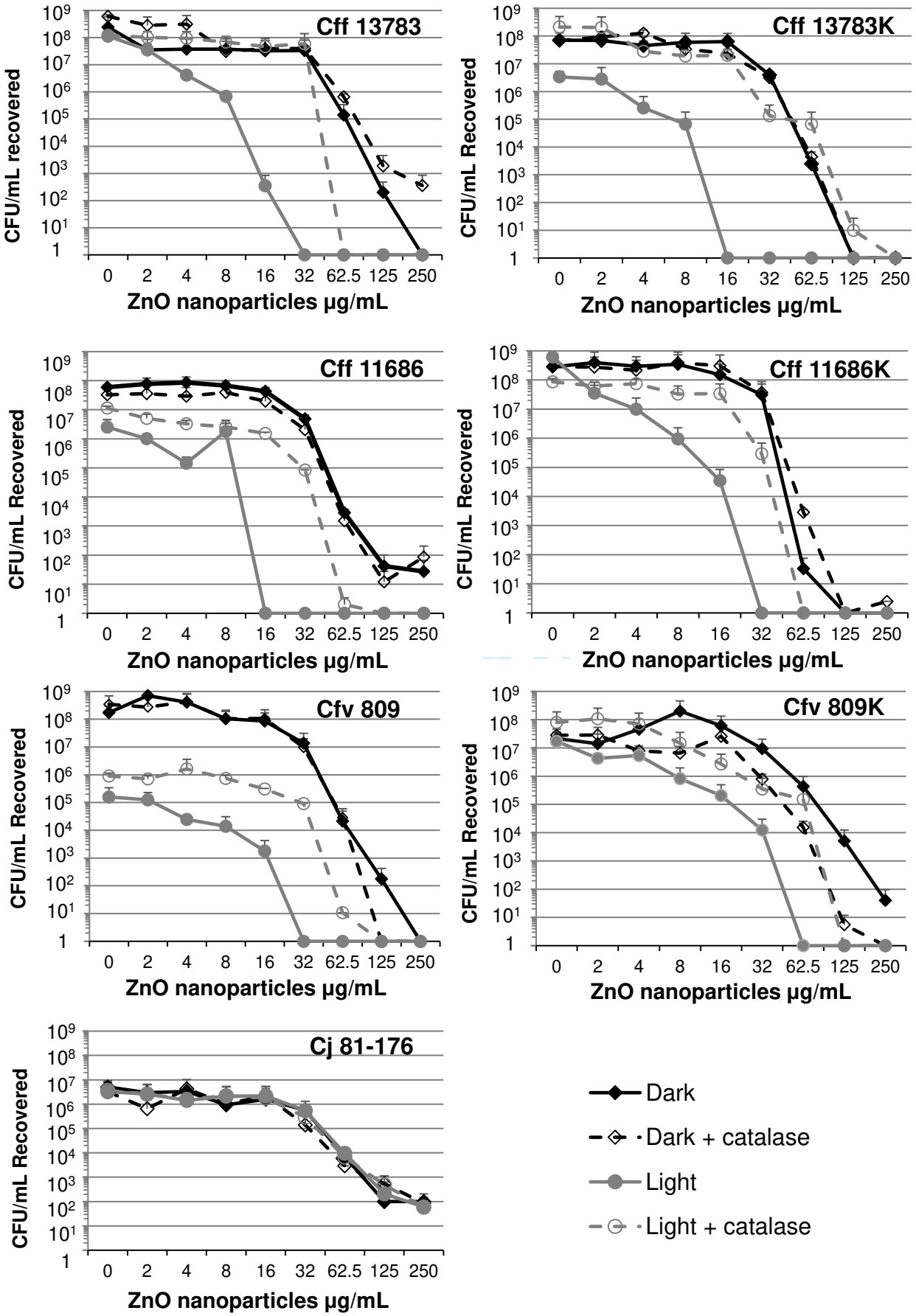
Cff 13783
Cff 13783K
Cff 11686
Cff 11686K
Cfv 809
Cfv 809K
Cj 81-176
CFU/mL recovered
CFU/mL Recovered
ZnO nanoparticles µg/mL
0 2 4 8 16 32 62.5 125 250
Dark
Dark + catalase
Light
Light + catalase

Figure 4. Photoactivation enhances ZnO nanoparticle activity towards C. fetus. MBC assays were conducted in duplicate 96 well plates incubated at 37℃ under microaerobic conditions. Following bacterial inoculation, one plate was incubated in the dark (Dark) and the duplicate plate was exposed to visible light for 30 min (Light) prior to incubation in the dark. Catalase (4 μg/mL) was included in replicate wells (Dark + catalase; Light + catalase). After 24 h exposure to ZnO nanoparticles, surviving bacteria were enumerated using viable plate counts. Data is presented as the mean + SD of at least 2 independent assays conducted on different days. Cff, C. fetus subsp. fetus; Cfv, C. fetus subsp. venerealis; Cj, C. jejuni. S layer deficient strains are indicated by the letter "K" following the strain number.

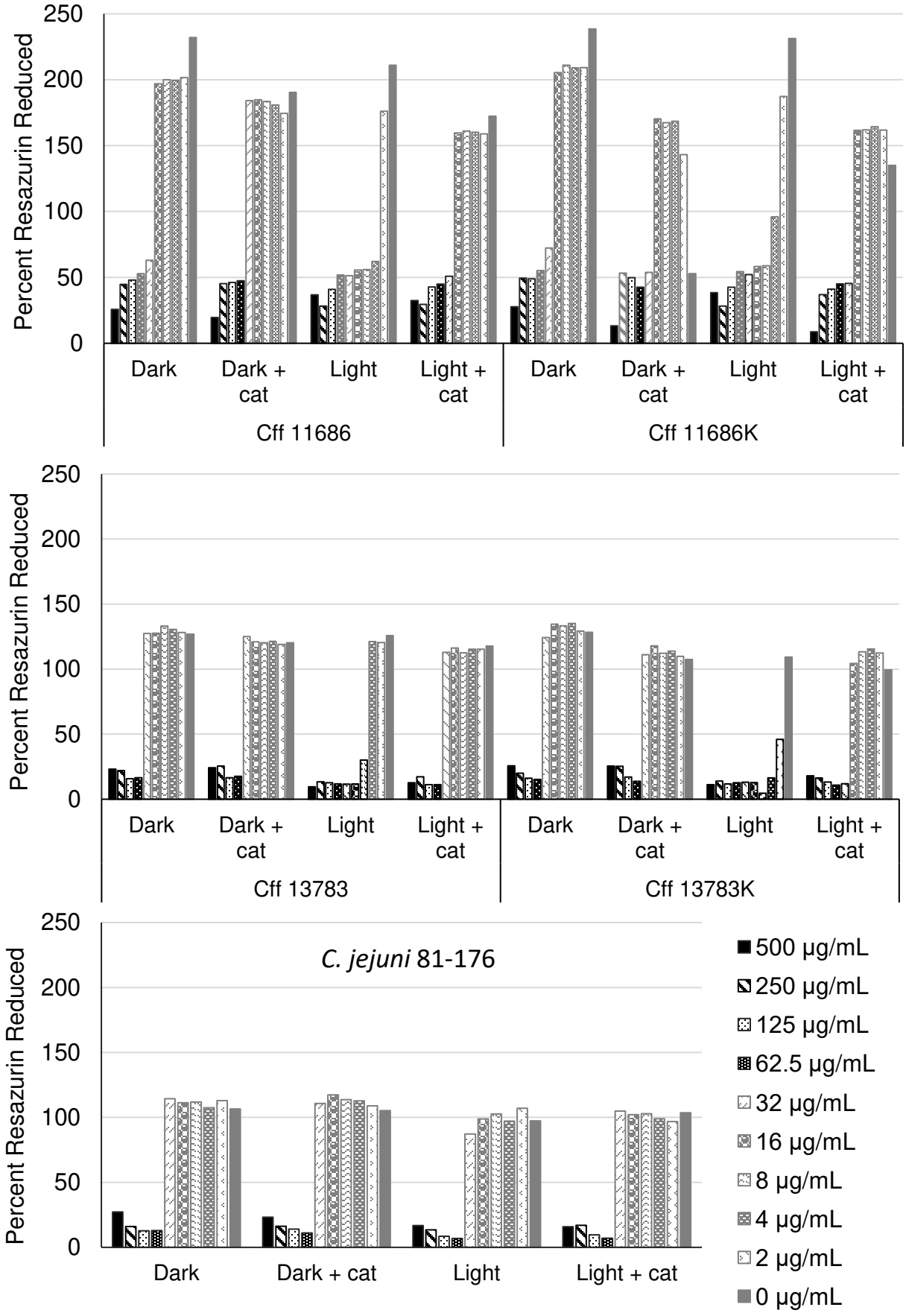
Percent Resazurin Reduced
250
200
150
100
50
0
Dark
Dark + cat
Light
Light + cat
Cff 11686
Cff 11686K
Cff 13783
Cff 13783K
C. jejuni 81-176
500 µg/mL
250 µg/mL
125 µg/mL
62.5 µg/mL
32 µg/mL
16 µg/mL
8 µg/mL
4 µg/mL
2 µg/mL
0 µg/mL

Figure 5. Zinc oxide nanoparticles inhibit bacterial metabolic activity. Resazurin reduction, an indicator of cell metabolic activity, was assessed after 24 h exposure to ZnO nanoparticles. Data shown is representative of 2 replicate assays. Dark bars indicate loss of metabolic activity (≤ 50% resazurin reduction). Grey bars indicate residual metabolic activity. Legend numbers in μg/mL.